



# Experimental demonstration of creep life improvement in welded joints through optimized welding conditions

Hitoshi Izuno<sup>1</sup> · Masahiko Demura<sup>1</sup> · Kenji Nagata<sup>2</sup> · Daisuke Abe<sup>3</sup> · Keisuke Torigata<sup>3</sup>

Received: 13 July 2025 / Accepted: 3 December 2025 / Published online: 30 January 2026  
© The Author(s) 2026

## Abstract

Creep tests were conducted on weld joints under welding conditions with high creep performance. 2 1/4Cr-1Mo steel, which is widely used in high-temperature components such as boilers and piping of power and petrochemical plants, was selected as the target material. The creep performance of weld joints is governed by the stress distribution in the fine-grained heat affected zone (HAZ) during welding, which in turn depends on the HAZ shape. In this study, we demonstrated that creep performance can be controlled by welding conditions. The welding conditions were determined using a tandem Bayesian model that linked welding conditions and creep life through HAZ shape factors. This framework is a probabilistic combination of two surrogate models: a Gaussian process that predicts the HAZ shape from welding parameters, and a Bayesian linear regression that estimates the rupture life. The search targets are the number of layers, layer thickness, and heat input. Long-life conditions that were 1.8 times longer than the maximum life of the initial training data were explored. Two other conditions were selected: standard welding conditions and short-life welding conditions. Welding and creep tests were performed, and the results of the creep tests were in the order of long > standard > short. The HAZ shapes reflected the differences in life, as expected from the welding conditions. In conclusion, it was proved that the creep life can be controlled by adjusting the welding conditions.

**Keywords** 2 1/4Cr-1Mo steel · Weld joint · Bayesian inference · Creep property · Welding condition · Heat affected zone · Inverse problem · Creep test

Recommended for publication by Commission X - Structural Performances of Welded Joints - Fracture Avoidance

✉ Masahiko Demura  
DEMURA.Masahiko@nims.go.jp

Hitoshi Izuno  
IZUNO.Hitoshi@nims.go.jp

Kenji Nagata  
NAGATA.Kenji@nims.go.jp

Daisuke Abe  
abe9500@ihi-g.com

Keisuke Torigata  
torigata7492@ihi-g.com

<sup>1</sup> Research Network and Facility Services Division, National Institute for Materials Science, Tsukuba, Japan

<sup>2</sup> Center for Basic Research On Materials, National Institute for Materials Science, Tsukuba, Japan

<sup>3</sup> Corporate Research and Development Division, IHI Corporation, Yokohama, Japan

## 1 Introduction

Weld joints of heat-resistant steels such as 2 1/4Cr-1Mo are known to fail due to creep rupture caused by Type IV damage, which initiates and grows creep voids in the fine-grained heat-affected zone (HAZ) of the base metal during welding [1–3]. 2 1/4Cr-1Mo steel is widely used in high-temperature components such as power plant boilers and petrochemical plant piping, which are exposed to elevated temperatures for extended periods. Improving the creep life of weld joints in these applications is a critical issue directly linked to enhancing the reliability of such equipment. The creep strength of the HAZ is significantly lower, and the creep strength of the simulated HAZ, where the thermal history during welding is reproduced for the base metal, decreases to approximately one-third to one-tenth that of the base metal. On the other hand, it has been reported that the creep rupture life of actual weld joints is longer than that of the simulated HAZ [4–6]. This discrepancy is believed to be attributed to the structural configuration of weld joints, where the HAZ, whose material

properties are different from the base metal, is sandwiched between the base metal and weld metal.

Several studies have investigated the creep life of weld joints by focusing on the geometrical configuration of the HAZ [7–15]. Regarding the sensitivity of creep rupture life to the HAZ inclination caused by changes in the bevel angle, experimental creep tests by Francis et al. [7] and Parker et al. [8], as well as computational analyses of creep damage by Koiwa et al. [9] and Tanner et al. [10], have reported a decrease in rupture life when the HAZ was inclined relative to the tensile axis. Additionally, Divya et al. [11] and Hashimoto et al. [12] investigated the effect of HAZ width in the tensile direction and reported a negative correlation with rupture life. Watanabe et al. [13] and Hongo et al. [14] performed creep damage analysis using FEM models that reproduce the actual complex weld geometry, emphasizing the importance of considering the three-dimensional stress distribution in evaluating creep damage. Based on these insights, Izuno et al. [15] compared creep damage analysis with experiments in simplified HAZ geometry, determined a creep damage model and its parameters for the HAZ, and demonstrated that deformation constraints caused by the differences in material properties between the base metal and HAZ reduce the equivalent stress within the HAZ. The stress reduction suppresses creep damage accumulation, which explains why actual weld joints exhibit longer creep life than the simulated HAZ.

Generally, the HAZ exhibits a complex geometry due to the intricate thermal cycles during welding. Assuming that the deformation constraint within such complex HAZ geometries can be described using geometric features extracted from the cross-sectional HAZ shape, it becomes feasible to explain the creep performance of weld joints through HAZ geometry. Since the thermal history of the weld zone is governed by welding heat input conditions, controlling the welding conditions during welding is expected to improve creep performance. Abe et al. [16] constructed a workflow to calculate the creep rupture life of weld joints under arbitrary welding conditions using the MInt system [17, 18], developed under the SIP program [19]. Izuno et al. [20] further used the outputs from this workflow to extract geometric features of HAZ cross-sectional shapes (HAZ shape factors). They proposed a tandem Bayesian model as an inverse problem framework to search for welding conditions that yield longer creep life. This tandem Bayesian model enabled the proposal of welding conditions that extend creep life by 12% compared to the longest among initial training data, with the calculations of only 0.02% of the total search space.

In this study, we proposed and experimentally validated long-life welding conditions under realistic welding conditions, aiming to improve the creep performance of weld joints of 2 1/4Cr-1Mo steel plates through optimal welding conditions. We assumed creep specimens to be extracted from groove weld joints. The tandem Bayesian model

searched across approximately 1.5 million combinations of layer thickness, heat input, and number of layers and proposed the optimal welding condition that was expected to have long creep life. Based on the results, three welding conditions of long creep life, standard welding, and short creep life were proposed. Weldments were prepared under these proposed welding conditions creep specimens were cut from them, and the results of creep tests were analyzed.

## 2 Method

### 2.1 Welding and creep testing

The cross-sectional configuration of the weldment used for experimental validation is shown in Fig. 1(a). A U-groove with a width of 6 mm and a depth of 9 mm was machined into a 2 1/4Cr-1Mo steel plate with a thickness of 12 mm and a length of 55 mm from the weld center line to the edge. The groove was filled by welding using gas tungsten arc welding (GTAW) in the flat position with 100% argon as the shielding gas, under various welding conditions within the ranges described below. The interpass dwell time was set to 40 s for each welding pass. The chemical compositions of the base metal and filler material are shown in Table 1.

The welding parameters targeted in the search included:

- (1) Number of layers: 3 to 9 layers (7 levels),
- (2) Layer thickness: 1, 2, 3 mm (3 levels),
- (3) Heat input: 1200, 1400, 1600, and 1800 J/mm (4 levels), as defined in the Goldak double-ellipsoidal heat source model.

As shown in Table 2, this resulted in approximately 1.5 million combinations of welding conditions. Preliminary tests confirmed that sound welds can be obtained within this range of conditions.

Cross-sectional images of the weldments were obtained by cutting perpendicular to the weld center line, polishing to a mirror finish, and etching with a hydrochloric acid–picric acid solution, followed by observation under an optical microscope (OM). From each weldment, creep specimens were cut from the region indicated by the red frame in Fig. 1(a), with a gauge length of 30 mm, in the form of square-bar specimens with gripping tabs. The shape of the specimens viewed from the plate surface is shown in Fig. 1(b). Tensile creep tests were conducted at 873 K and 100 MPa in accordance with JIS Z 2271:2010. Ruptured specimens were cut perpendicular to the weld line, embedded in resin, and subjected to the same surface treatment as weldments, before OM observation to obtain cross sectional images.

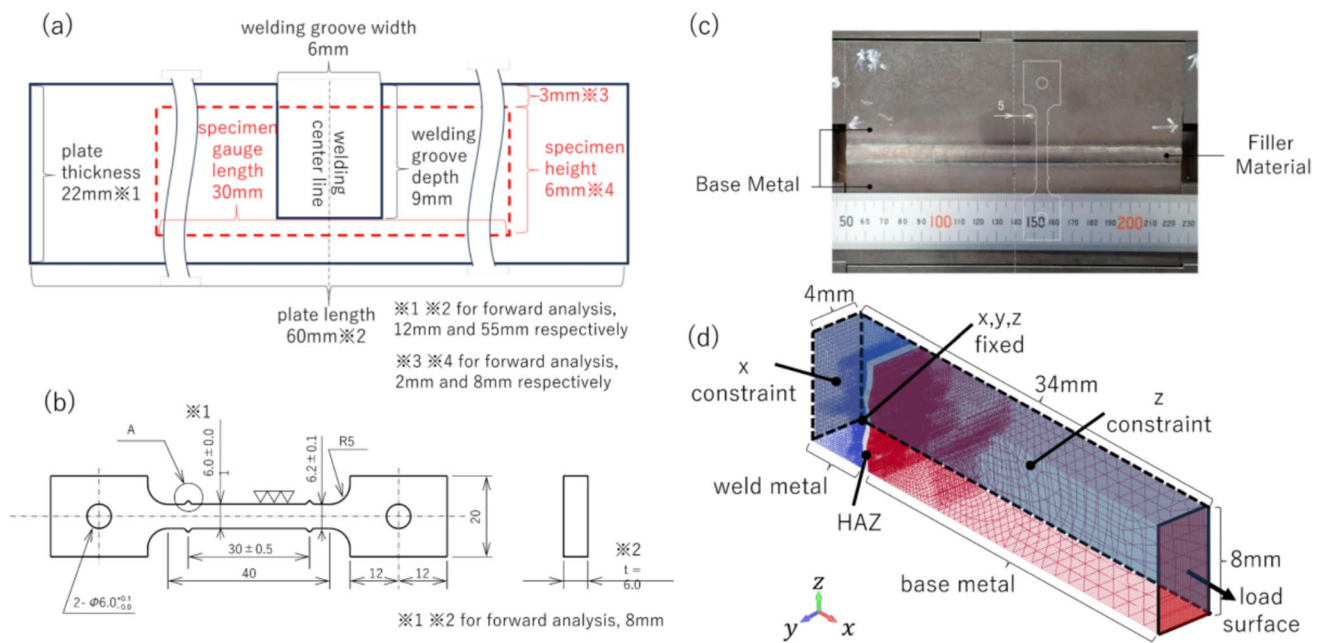


**Fig. 1** (a) Schematic diagram of the welding body and U-welding groove, and test specimen gage section extraction position, shown in red dashed line, (b) rectangular column creep test specimen dimension, (c) schematic figure of the test specimen extraction direction

from the welding body and (d) FEM geometry and constraint conditions for creep damage analysis. The FEM model shown in (d) corresponds to the 8 mm-high region indicated by the red box in (a), which was extracted for creep damage analysis

**Table 1** Chemical composition of base metal and filler materials for welding specimens of 2 1/4Cr1Mo steel

Composition (wt %)	C	Si	Mn	P	S	Cu	Ni	Cr	Mo	Nb	V	Al	Ti
Base Metal	0.14	0.10	0.55	0.007	0.002	0.03	0.03	2.38	1.05	0.00	0.00	0.037	0.00
Filler Material	0.12	0.30	0.70	0.005	0.007	0.23	0.03	2.30	1.05	-	-	-	-

## 2.2 Forward analysis method

Forward analysis followed the workflow proposed in previous research [16], comprising three steps: heat conduction analysis during welding, HAZ identification, and FEM-based creep damage analysis. First, for each welding condition, the maximum temperature distribution during welding was calculated via heat conduction analysis. Next, the HAZ region was defined as the area where the maximum temperature ranged between 775 °C and 875 °C, based on prior studies [16]. Finally, a FEM model incorporating the HAZ geometry was constructed, and creep damage analysis was conducted. In this study, based on the abovementioned definition of a HAZ, FEM models were constructed in which the region with a maximum temperature of 875 °C or higher was the weld metal, the region between 775 °C and 875 °C as the HAZ, and the region below 775 °C as the base metal. Since we assumed that specimens were cut from the weldments (see Fig. 1(a)), additional computation steps were included to account for this configuration. Creep damage analysis was performed using a 3D quarter-symmetry model shown in

Fig. 1(d), simulating test conditions of 873 K and 100 MPa. Starting from the symmetry plane set at the weld center line of the FE model, material properties were assigned to the weld metal, HAZ, and base material, in that order.

Detailed parameters for the heat conduction and creep damage analyses are provided in Appendix 1. The forward analysis workflow was implemented on the MInt platform. The heat conduction analysis was performed by Code\_Aster [21], and FEM analysis was performed by FrontISTR [22]. The creep deformation law was the Norton–Arrhenius law, and the creep damage model followed the time exhaustion rule using the Huddleston stress as the scalar stress [23].

## 2.3 Optimization method

Two modules of forward analysis, heat conduction analysis and creep damage analysis were replaced with surrogate models, which were probabilistic machine learning models connected via HAZ shape factors. This approach, referred to as the tandem Bayesian model [20], was used for optimization. The HAZ shape factors are descriptors of geometric

**Table 2** Number of input variables, number of conditions, number of initial conditions, achieved maximum rupture life, number of rounds and steps, number of added learning data, and search efficiency, for each number of layers

layer	set	number of weld- ing parameter	number of search condition	number of initial training data	achieved rup- ture time(h)	step	round	number of added train data			ratio of the number of added train data per number of search condition (%)	
								for GP	for BL	Tr could be calculated		
												candidate
3		3	64	4	540	11	5	37	27	12	58.0	42.2
4		8	4096	8	<b>630</b>	42	8	132	46	33	3.22	1.10
5		10	46080	11	610	58	8	188	56	27	0.407	0.120
6		12	204800	12	430	100	10*	423	85	6	0.207	0.0500
7		14	458752	13	170	85	9	340	87	2	0.0740	0.0190
8	1	8	65536	10	270	82	10*	358	94	1	0.546	0.143
	2	8	65536	10	380	58	10*	226	88	2	0.345	0.134
	3	8	65536	10	270	90	10*	465	91	3	0.710	0.139
	4	8	65536	10	-	3	2	20	10	0	0.0305	0.0153
	5	8	65536	10	280	130	10*	548	97	22	0.836	0.148
	6	8	65536	10	250	5	3	21	12	1	0.0320	0.0183
	7	8	65536	10	-	5	2	20	10	0	0.0305	0.0153
	8	8	65536	10	98	3	2	20	10	1	0.0305	0.0153
9		9	262144	12	-	6	3	42	8	0	0.0160	0.00305
summary			1500224	140	<b>630(max)</b>			2840	721	110	0.189	0.0481
* terminated at 10 round												

features for the HAZ, which is assumed to have high explanatory power for rupture life.

The surrogate model for heat conduction analysis was constructed using Gaussian Processes (GP) with welding conditions as input and HAZ shape factors as output. The surrogate model for creep damage was built using Bayesian linear regression (BL), with HAZ shape factors as input and rupture life as output. Model selection [24] was applied to determine the best regression model from all 127 possible combinations of seven HAZ shape factors. The best model, selected by the maximum marginal log likelihood, served as the surrogate model. For model selection, both input and output variables were normalized.

By probabilistically linking the GP and BL, the Figure of Merit (*FoM*) was defined as the probability that any given welding condition would exceed the target rupture life among the training data. Details of the surrogate model construction and *FoM* computation are described elsewhere [20].

A schematic figure of the tandem Bayesian optimization process using the forward model is shown in Fig. 2. First, forward analysis was performed on initial welding conditions to build the surrogate model. Based on *FoM*, the top 10 candidates were selected for additional training data, from the search space. Heat conduction analysis was conducted for candidates not already included in the GP training data, and the GP was updated with the new data. The top 10 candidate selection and model updating cycle was repeated until all candidates had been included in the GP training data, thereby optimizing the GP. Once the GP was optimized, the BL model was subsequently updated. Creep

damage analyses were performed for candidates not included in the BL training data, and the results were used to update BL. If a longer rupture life than the current target rupture life was found, the target rupture life was also updated. This cycle of GP optimization and BL update was repeated until all candidates were included in the BL training data. This method reduces the number of relatively expensive creep damage analyses by first optimizing GP. The GP updates were referred to as steps, and the BL updates as rounds. The process was terminated if 10 rounds were reached without convergence.

Since the combination of explanatory variables varies with the number of layers, separate surrogate models were constructed for each number of layers. Figure 3 illustrates this approach. For example, with 3 layers, the U-groove must be filled with three 3 mm layers, resulting in a 3-dimensional input space comprising only the heat inputs per layer. With 4 layers, numerous combinations of layer thicknesses are possible, so both thicknesses and heat inputs per layer were used as variables, yielding an 8-dimensional input space. Therefore, the search space was divided according to the layer thickness, and tandem Bayesian model was performed independently for each search space. For 8 layers, exceptionally, the number of thickness combinations is limited to 8 (one 2 mm layer and seven 1 mm layers), so only heat inputs per layer (8 variables) were considered for 8 sets of different thickness combinations. Table 2 summarizes the dimensionality of explanatory variables for each layer count.

The derivation of variable combinations and corresponding condition counts per number of layers is provided in Appendix 2. The initial GP training data consisted of

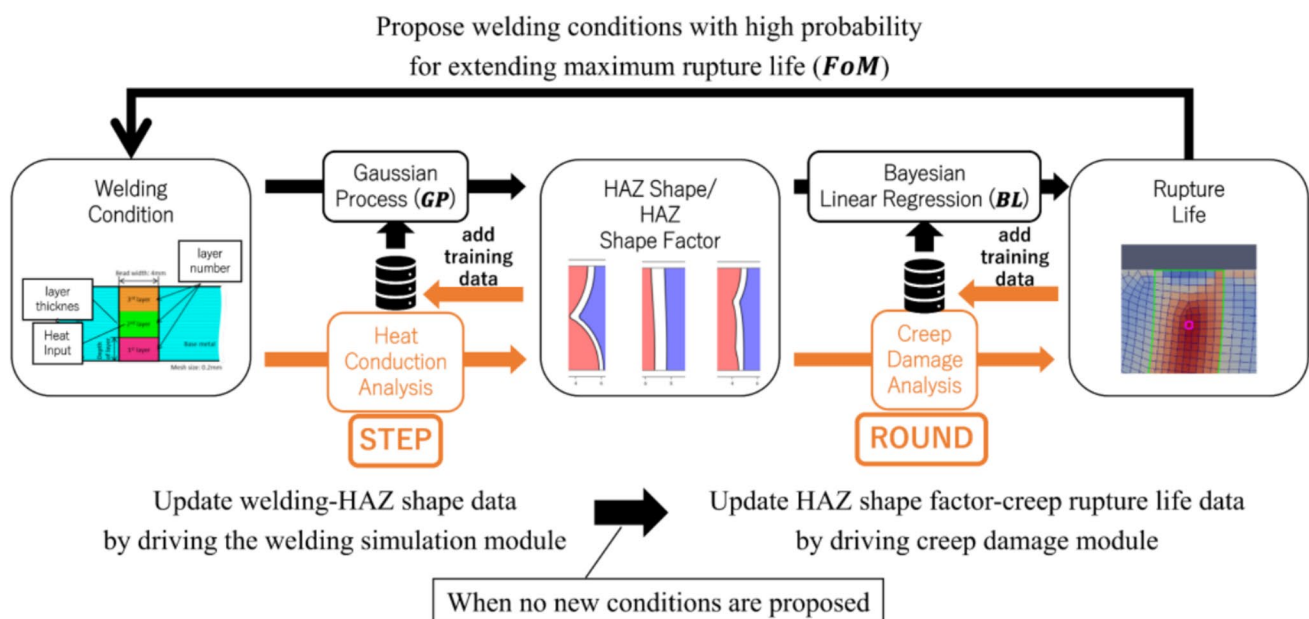
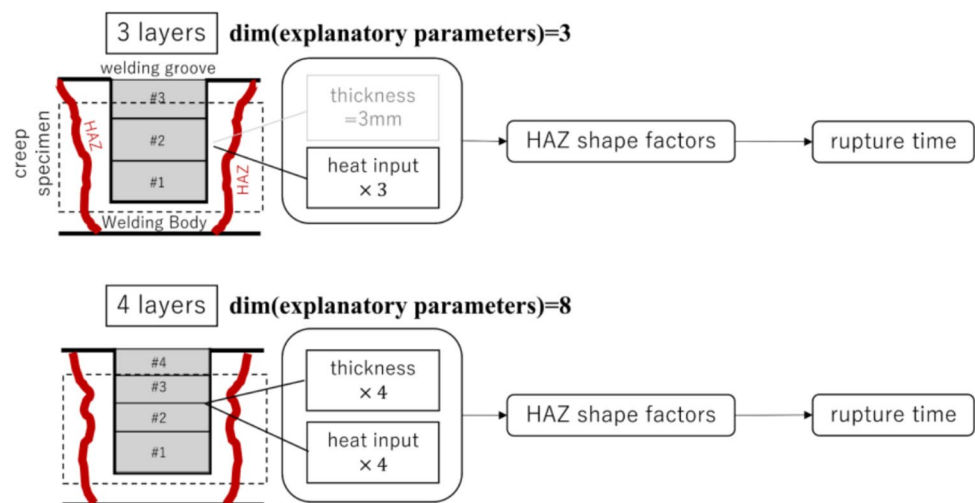


**Fig. 2** Schematic diagram of a tandem Bayesian model in which the forward calculation is transferred to corresponding surrogate model



**Fig. 3** Schematic diagram of providing individual surrogate models for welding heat conduction analysis according to the number of layers



randomly selected samples, proportional to the logarithm of the search condition count per each number of layers (total of 140 conditions; see Table 2). The initial BL model was built using all initial GP training data, which were common across the numbers of layers. The initial target rupture life was set to the longest rupture life among the BL initial data.

### 3 Result and discussion

#### 3.1 Results of initial conditions

Forward analysis of the initial welding conditions revealed that, in many cases, elements with damage = 1 appeared very early in the analysis. These elements were adjacent to the so-called triple junctions, i.e., the intersections between the HAZ and either the weld metal or the base metal, which are located along the free surfaces of the FEM model. At these triple junctions, elements with differing material constants share a face in contact with the free surface, sometimes leading to stress singularities, where stress theoretically diverges to infinity [25, 26]. These are known as singular stress fields, which are difficult to handle accurately within FEM frameworks.

However, if the stress divergence due to a singular stress field remains highly localized, the resulting damage is unlikely to propagate significantly into surrounding regions. Damage induced by singular stresses is confined to a narrow zone and does not affect the overall damage distribution over time. Therefore, it is unlikely that such localized damage would lead to overall creep rupture. In fact, in actual creep tests of welded joints, no immediate creep rupture due to stress dissipation at the triple junction after loading has been reported. Consequently, it can be assumed that damage caused by stress singularities at triple junctions does not contribute to creep rupture of a specimen.

Based on this assumption, we excluded damage determined to arise from singular stress fields at triple junctions. The evaluation method is as follows: using time-series data of damage distribution from the FEM analysis, we judged damage to be due to singular stress fields if elements with damage = 1 near triple junctions did not expand spatially (Fig. 4(a)). In such cases, this damage was ignored, and the rupture life was defined by the time at which a damage = 1 element appeared in a region related to the triple junctions. Conversely, if the damage = 1 elements expanded over time from the triple junction to surrounding regions (Fig. 4(b)), rupture life could not be determined due to ambiguity in classification, and these cases were excluded from the training data.

Applying this classification method, rupture life could be determined for 10 of the 140 initial conditions. Combined with 60 datasets calculated in previous work [20], the total initial training data amounted to 70 conditions. The initial target rupture life was set at 350 h, the longest life among the new 10 conditions.

To avoid selecting conditions where rupture life cannot be determined during optimization, a probabilistic classifier was developed to estimate the likelihood that the rupture life is determinable. The output of the classifier was multiplied by the *FoM* for screening. Thus, candidate conditions for additional training data were selected based on the joint probability of exceeding the target life and having a determinable rupture life. Further details of the classification method are provided in Appendix 3.

#### 3.2 Optimization Results

In Table 2, for each number of layers (or sets for 8-layer combinations), the obtained maximum rupture life, the number of GP steps and BL rounds, execution counts for heat conduction analysis and creep damage analyses, and

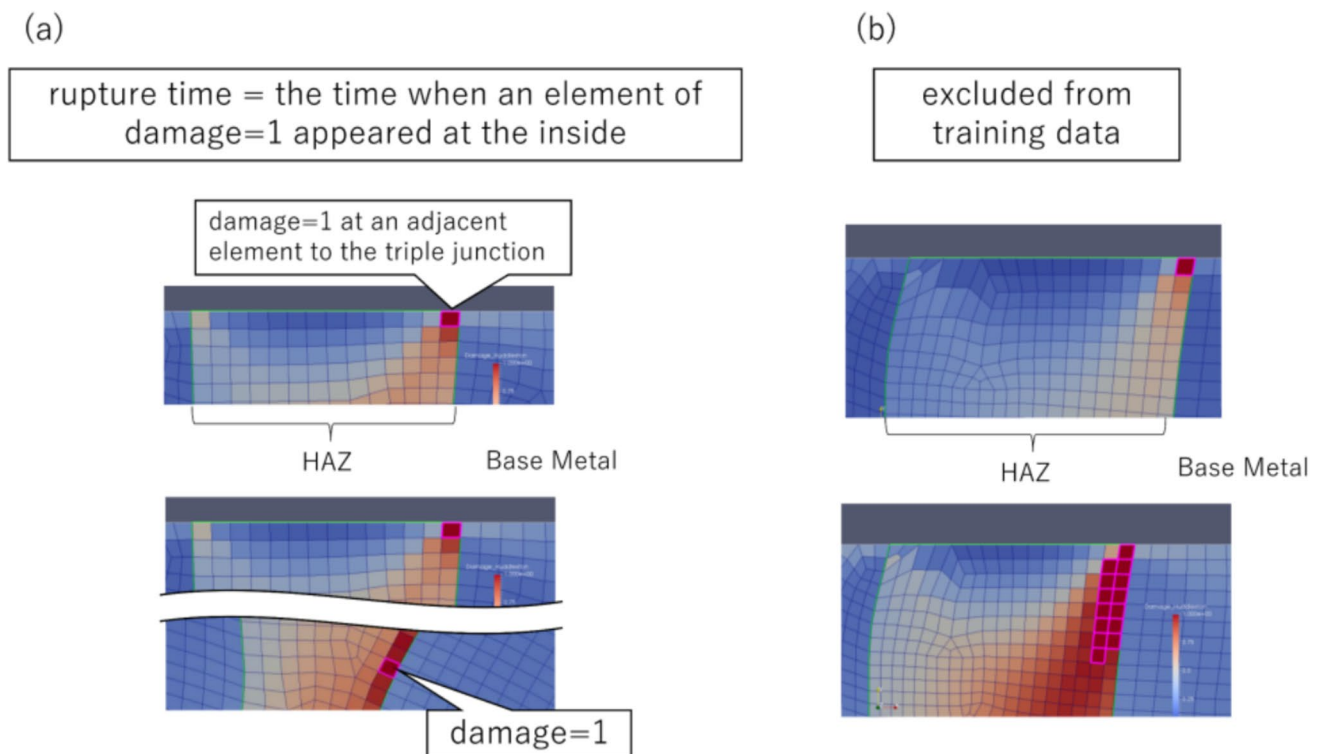


**Fig. 4** Schematic figure of a framework for determining rupture life depending on whether an area of damaged elements extends from the triple point. (a) the case which rupture life can be obtained and (b) exclude from training data

their percentages relative to the total search condition count for each number of layers are summarized. For the 4-layer case, the longest rupture life reached 630 h, that is 1.8 times longer than the initial target, which is the longest among all conditions. Optimization required 42 GP steps and 8 BL rounds. Forward computations included 132 heat conduction analyses (3% of 4096 total conditions) and 46 creep damage analyses (1%), demonstrating efficient identification of promising conditions. Among the 46 creep analyses, rupture life was successfully determined in 33 cases (about 72%), indicating high accuracy of the classifier.

Another favorable result was obtained for 5-layer conditions, with a maximum rupture life of 610 h. Although the 5-layer space included 46,080 conditions—nearly 10 times more than the 4-layer case—the percentage of forward analyses was even lower (heat conduction: 0.41%, creep: 0.12%), further confirming the efficiency of the tandem Bayesian model. In contrast, for 8-layer set 5, optimization continued until round 10 without identifying a rupture life exceeding the initial target. Despite executing 0.84% of heat conduction and 0.15% of creep damage analyses, the search was terminated, suggesting that viable long-life conditions may be absent or extremely rare in this space.

Figure 5(a) shows rupture life distributions for training data added to the BL by layer count. Gray dots represent data points, and black crosses indicate the longest life

in each number of layers. The initial target life is shown by the dashed line. For layer counts of 3–6, many added data points exceed the initial target. In contrast, for layer counts of 7 and above, most data fall below the initial target, suggesting that a higher number of layers leads to lower likelihood of identifying long-life conditions. This may be attributed to the fact that an increase in the number of layers leads to each layer becoming thinner, and in each thinner layer, more heat input per volume is received, which causes an increase in HAZ width and thus reduces creep performance.

Figures 5(b) and 5(c) illustrate how data are added across rounds for 4-layer and 8-layer set 5 cases. Black dots indicate new data added in each round, gray dots show previously added data, and small gray dots represent initial data. In the 4-layer case, many data points already exceeded the target in round 1, and target rupture life updates continued in subsequent rounds, indicating that the surrogate model was well-optimized initially and further enhanced through learning from long-life conditions. In contrast, in set 5 with 8 layers, even as the round progressed, the rupture life of the additional learning data remained at the same level as that of the initial training data, and no conditions exceeding the target rupture life were added to the training data. In other words, the surrogate model was not optimized in the direction of finding long-life conditions (i.e. on the utilization side).

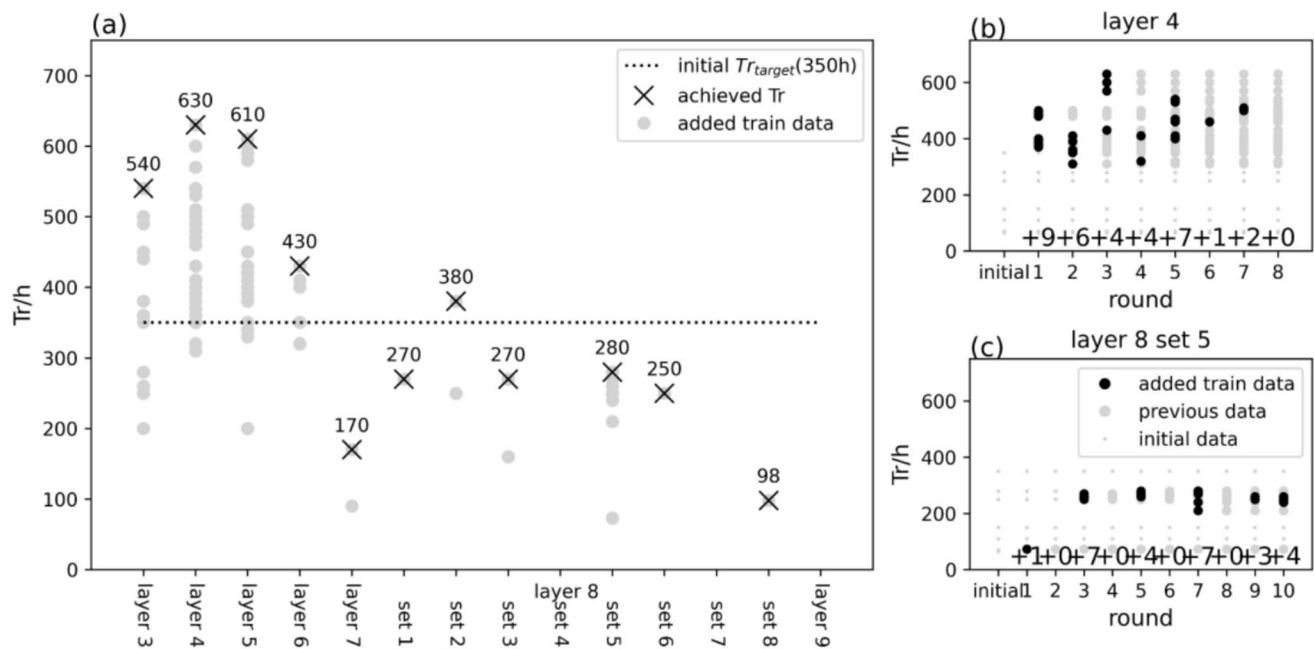


**Fig. 5** (a) Result of adding training data for Bayesian linear regression by number of layers. X marks are the achieved maximum rupture time for each number of layers. (b) and (c) The progress of adding training data by round for layer 4 and layer 8 set 5

Figure 6 shows results from regression model selection in the final round for the 4-layer case. Figure 6(a) is a heatmap of regression coefficients from the top 20 models of posterior probability. Figure 6(b) shows the selection frequency for each HAZ shape factor. The best model is shown on the left side of Fig. 6(a), with a posterior probability of 32.7%, which is the highest, and it best explains the final learning data in the four-layer stack, which contains many long-life

conditions. The best model included four HAZ shape factors: average HAZ width (width\_ave), maximum HAZ width (width\_max), HAZ length (bd\_ave), and maximum HAZ width at the free surface (FS\_HAZ\_W), all of which had high explanatory power for rupture life. In fact, all of these factors showed an adoption rate of 50% or more and are important explanatory variables across models.

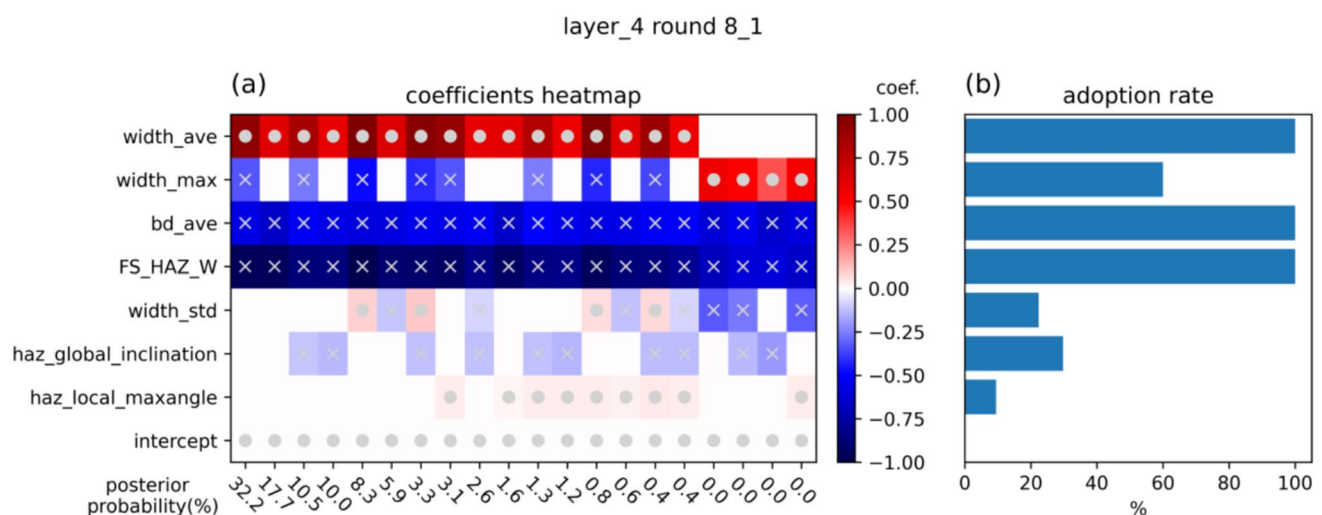


**Fig. 6** (a) Coefficient heatmap of HAZ shape factors for top 20 candidates of the model selection of Bayesian linear regression at 4-layer, final round. Gray circle denotes the coefficient is plus, and cross mark

denotes the coefficient is minus. (b) Adoption rates of all Bayesian linear regression for each HAZ shape factor of the model selection, at the final round for 4-layer



Notably, among the three HAZ shape factors, the maximum width of the HAZ, the length of the HAZ, and the maximum width of the free surface of the HAZ were also selected as explanatory variables for the best BL model in previous studies [20]. As shown in Fig. 6(a), the regression coefficients for these three factors are all blue, which means they are negative. This indicates that creep deformation of the HAZ is effectively constrained by the base and weld metal. The creep strength of HAZ is low and it has a tendency to accumulate damage, but it is constrained by the base metal and weld metal, which have higher creep strength. Therefore, the rupture life of the weld joint is longer than that of the HAZ alone but shorter than that of the base metal. To achieve effective deformation constraint, the width of the HAZ should be as narrow as possible, and the shape of the HAZ should be perpendicular to the tensile direction.

On the other hand, average HAZ width was not selected in previous studies, and was selected for the first time in the present study as it had a high explanatory power. It is noteworthy that the regression coefficient is positive (shown red in Fig. 6(a)). Considering this together with the fact that the regression coefficient for the maximum HAZ width is negative, this means that it is advantageous for rupture life to minimize the maximum HAZ width while reducing overall width variation. In other words, a smooth HAZ interface is required. In conclusion, it is considered that the Bayesian linear regression model selection was performed to establish long creep life conditions by suppressing the maximum HAZ width while maintaining a smooth HAZ with a shape perpendicular to the tensile axis.

### 3.3 Experimental validation via creep testing

Three welding conditions were selected for experimental validation, as shown in Table 3. The long creep life condition ("Long") was the 4-layer weld setting that achieved 630 h in simulation. It used moderate layer thicknesses in the initial layers and high heat input, while the final layer employed lower heat input to aim at creating a vertical HAZ profile. The "Normal" condition was a 5-layer weld that was considered to enable stable welding, based on observations of actual welding, with calculated rupture life of 310 h. It used moderate thickness and heat input for each layer, which were average. In addition, assuming that the final layer should be filled completely, the thickness of the final layer was selected to be moderate. The "Short" condition was an 8-layer weld that had the shortest predicted life (71 h). In the Short condition, the thickness of the second and subsequent layers was set to the minimum value. On the other hand, the heat input was high overall, resulting in a wider HAZ width. Furthermore, it was assumed that the HAZ moved away from the

**Table 3** Welding conditions, obtained rupture times for forward calculation, creep test, full-forward and creep only, shape factors for the real HAZ shape and full-forward, for Long, Normal and Short testing conditions

candi- date	number of lay- ers	rupture time by forward calcula- tion (h)	welding conditions	layers								rupture time(h)		width max(mm)		bd ave		
				1	2	3	4	5	6	7	8	creep test	full- for- ward	creep- only	real HAZ shape	full- forward	real HAZ shape	full- forward
Long	4	630	thickness (mm)	2	2	3	2	-	-	-	-	501.0	620	320	0.771	0.416	1.037	1.028
			Heat Input (J/mm)	1800	1800	1600	1200	-	-	-	-							
Normal	5	310	thickness (mm)	2	2	2	1	2	-	-	-	411.7	570	210	0.931	0.464	1.071	1.015
			Heat Input (J/mm)	1800	1600	1800	1800	1400	-	-	-							
Short	8	71	thickness (mm)	2	1	1	1	1	1	1	1	340.1	<300	160	1.112	0.676	1.082	1.062
			Heat Input (J/mm)	1200	1400	1200	1600	1800	1600	1800	1600							

groove at positions close to the free surface, resulting in the HAZ shape tilting in the tensile direction.

Weldments were fabricated for these three conditions, and test pieces were cut out as shown in Fig. 1(c) and creep tests were performed. The obtained rupture lives were 501.0 h for Long, 411.7 h for Normal, and 340.1 h for Short. The order of rupture lives obtained from experimental (Long > Normal > Short) matched the model's predictions. Notably, the Long condition outlasted the Normal by ~22% and the Short by ~47%. Despite only a one-layer difference between Long and Normal, the change in welding conditions had a significant impact. However, discrepancies were observed between simulation and experiment: the life of Long was about 20% shorter than predicted, while that of the Short was about 5 times longer. These discrepancies are discussed in the following subsection.

The microstructural features of the heat-affected zone were first examined for the Long condition, as shown in Fig. 7. Figure 7(a) shows a low-magnification OM image of the weldment (macro observation), in which the black rectangle indicates the region that includes the HAZ. Figure 7(b) presents a higher-magnification OM image of this region, where three black rectangles correspond to (c) the coarse-grained heat-affected zone (CGHAZ), (d) the fine-grained heat-affected zone (FGHAZ), and (e) the base metal

(BM). Further higher-magnification images reveal that the heat-affected zone can be divided into two distinct regions: CGHAZ and FGHAZ. The FGHAZ exhibits a finer grain structure than the BM. Since the FGHAZ is finer than both the surrounding CGHAZ and BM, it appears as a darker-contrast region in the optical micrographs. Therefore, in low-magnification OM images, the dark-contrast region can be identified as the FGHAZ. In Figs. 7(a) and (b), the boundaries between the CGHAZ and FGHAZ and between the FGHAZ and BM are indicated by red and white lines, respectively, following this identification.

Low-magnification OM images of the weldments are shown in Fig. 8(a–c) for the Long, Normal, and Short conditions, respectively. In these figures, red and white lines mark the boundaries between CGHAZ–FGHAZ and FGHAZ–BM, respectively. These boundaries were identified based on optical contrast differences, as established by the higher-magnification observations described above. The red-hatched area indicates the creep specimen region. The Long condition yielded a vertical and narrow FGHAZ, whereas the Normal and Short conditions exhibited wider and more inclined FGHAZs, with the Short condition being the most extreme. These results qualitatively match the expected HAZ shapes based on the welding parameters.

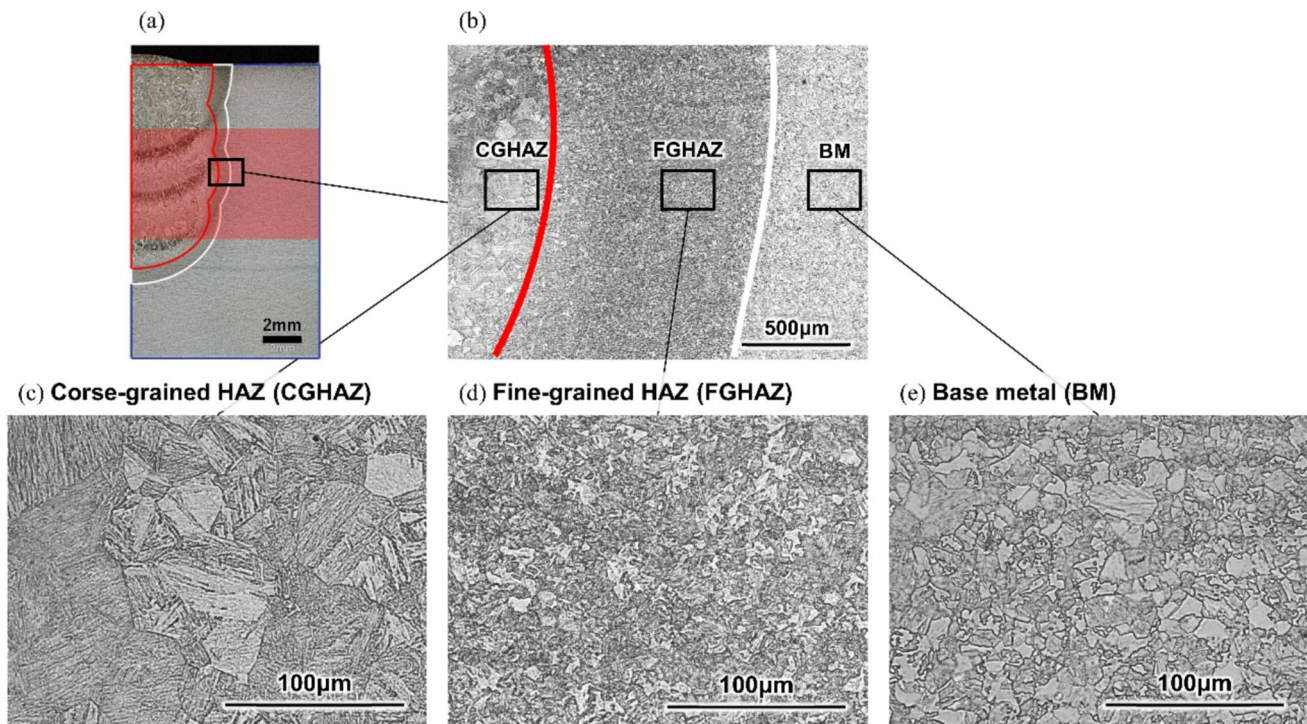


**Fig. 7** Optical micrographs of the heat-affected zone in the Long condition. (a) Low-magnification OM image (macro observation) of the weldment showing the overall weld joint; the black rectangle indicates the region including the heat-affected zone. (b) Higher-magnification OM image of the region shown in (a), where three black rectangles correspond to (c) coarse-grained heat-affected zone

(CGHAZ), (d) fine-grained heat-affected zone (FGHAZ), and (e) base metal (BM). (c–e) Higher-magnification OM images of each corresponding region. Red and white lines in (a) and (b) indicate the boundaries between CGHAZ–FGHAZ and FGHAZ–BM, respectively

**Fig. 8** OM cross-sectional macro figure of the weld joint for (a) Long, (b) Normal and (c) short condition, and of the ruptured specimen for (d) Long, (e) Normal and (f) Short condition. Red and white lines in (a), (b) and (c) indicate the HAZ boundary between weld metal and base metal respectively and red hatch areas show the gauge area of creep test specimens

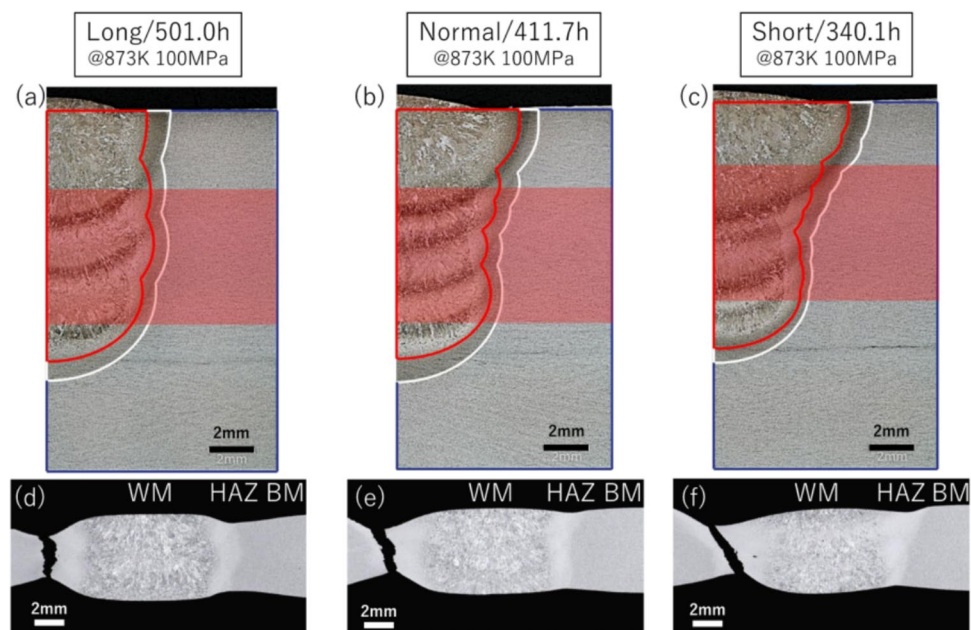


Table 3 summarizes maximum HAZ width and length from the extracted regions. Maximum width was about 0.8 mm for Long, about 0.9 mm for Normal, and about 1.1 mm for Short, supporting the negative effect of HAZ width on rupture life. A similar trend was observed for HAZ length. As shown here, the relationship between the HAZ shape factor predicted by Bayesian linear regression and creep rupture life was experimentally confirmed.

Cross-sectional images of the fracture surfaces of ruptured specimens are shown in Figs. 8(d–f). Each is oriented with the top of the weldment facing upward. In addition, assuming that the HAZ shape is symmetrical, the image is flipped left and right as appropriate so that the ruptured side is located on the left side. A bright-contrast HAZ is located on both sides of the rough weld metal in the center, with low-contrast base metal further outside. All rupture occurred within the HAZ, adjacent to the base metal, which indicates Type IV failure. Rupture surface for Long was nearly perpendicular to the tensile axis, whereas Normal and Short were inclined, with greater inclination in Short. These trends corresponded to the observed HAZ geometry, suggesting that the rupture life was strongly influenced by HAZ shape.

Thus, experimental creep tests validated that the predicted rupture life order matched the creep test results. The results could be interpreted using the Bayesian linear regression model and HAZ shape factors, demonstrating that welding conditions influence HAZ shape, and HAZ shape influences creep rupture life. The combined approach of forward modeling and Bayesian optimization proved capable of designing long-life welding conditions validated with real creep test.

### 3.4 Comparison between forward analysis and creep testing

A discrepancy was observed between the rupture life obtained from the creep test and that predicted by forward analysis. To investigate the reason, it was first necessary to reconcile differences in the assumptions between the experiment and the simulation. In actual welding, due to practical constraints, the plate thickness used to prepare the U-groove weld joint was changed from 12 to 22 mm, and the distance from the weld line to the plate edge was extended from 55 to 60 mm (Fig. 1(a)). Additionally, due to limitations of the testing jig for the creep test, the specimen gauge section was reduced by 1 mm on both the top and side surfaces, resulting in a 6 mm × 6 mm cross section (Fig. 1(b)). The forward analysis was executed again to reflect these actual conditions.

Furthermore, the forward analysis consists of two calculations, welding heat conduction analysis and creep damage analysis. It was necessary to separately evaluate how accurately each simulation reproduced the actual HAZ and creep rupture behavior. For this reason, two types of forward analyses were conducted: the first, referred to as full-forward, included both the heat conduction and creep damage analyses based on input welding conditions; the second, referred to as creep-only, used the actual HAZ geometry obtained from the cross-sectional micrographs in Figs. 8(a–c) and performed creep analysis only.

Table 3 summarizes the results of the creep damage analysis for both full-forward and creep-only simulations. In both cases, the predicted rupture lives were within a range



of 0.5 to 2 times the experimental values, and the relative trends in rupture life were preserved. However, the absolute prediction accuracy of rupture life was low for both methods. Moreover, systematic differences were observed. In the full-forward analysis, rupture life was overestimated, 620 h for Long and 570 h for Normal, exceeding the corresponding creep test results by 120 h and 160 h, respectively. For Short, the rupture life could not be determined under the defined criteria, but the damage region expansion from the triple junction into the HAZ began significantly after 300 h. Regarding this time as a benchmark, the result was 40 h shorter than the actual test. In contrast, the creep-only analysis yielded rupture lives of 320 h for Long, 210 h for Normal, and 160 h for Short, each 180 h, 200 h, and 180 h shorter than the test results, respectively. Overall, excluding the undeterminable case, the full-forward analysis tended to overestimate, while the creep-only analysis tended to underestimate the creep rupture life.

First, the accuracy of HAZ geometry reproduction in the heat conduction analysis was evaluated. Figure 9 compares the full-forward HAZ shape (black solid lines) with the actual HAZ shapes shown in Figs. 8(a–c) (gray dashed lines). The horizontal axis represents the distance from the weld center line, and the vertical axis represents the thickness from the top edge of the weldment plate. The left-side shaded region in each figure indicates the groove area, subdivided according to

layer thickness, and the heat input for each layer is annotated. In the full-forward models, the HAZ geometry for the Long condition stood vertically from the groove bottom. In contrast, the Normal and Short conditions showed that the HAZ was inclined toward the base metal as it approached the free surface. The horizontal position of the HAZ from the groove edge also showed little discrepancy. The undulations of the HAZ interface associated with individual layers were well reproduced for Long and Normal, except for Short, where the high number of layers made them less distinct. These trends qualitatively matched the actual HAZ geometries. However, the HAZ widths predicted by full-forward analysis were obviously narrower than the actual measurements for all three conditions. As shown in Table 3, the maximum HAZ widths in the simulation were 0.4 mm for Long, 0.5 mm for Normal, and 0.7 mm for Short, approximately 0.3 to 0.5 mm narrower than the actual values. Since narrower HAZ widths tend to increase the predicted rupture life, this underestimation of width likely explains the overprediction observed in the full-forward analysis.

Next, the creep-only analysis, which used the actual HAZ geometry, consistently predicted shorter rupture lives than observed in the real creep test. This discrepancy is likely due to the inaccuracies in the material properties assumed in the creep damage model. The deformation constraint within the HAZ is primarily governed by the mismatch in

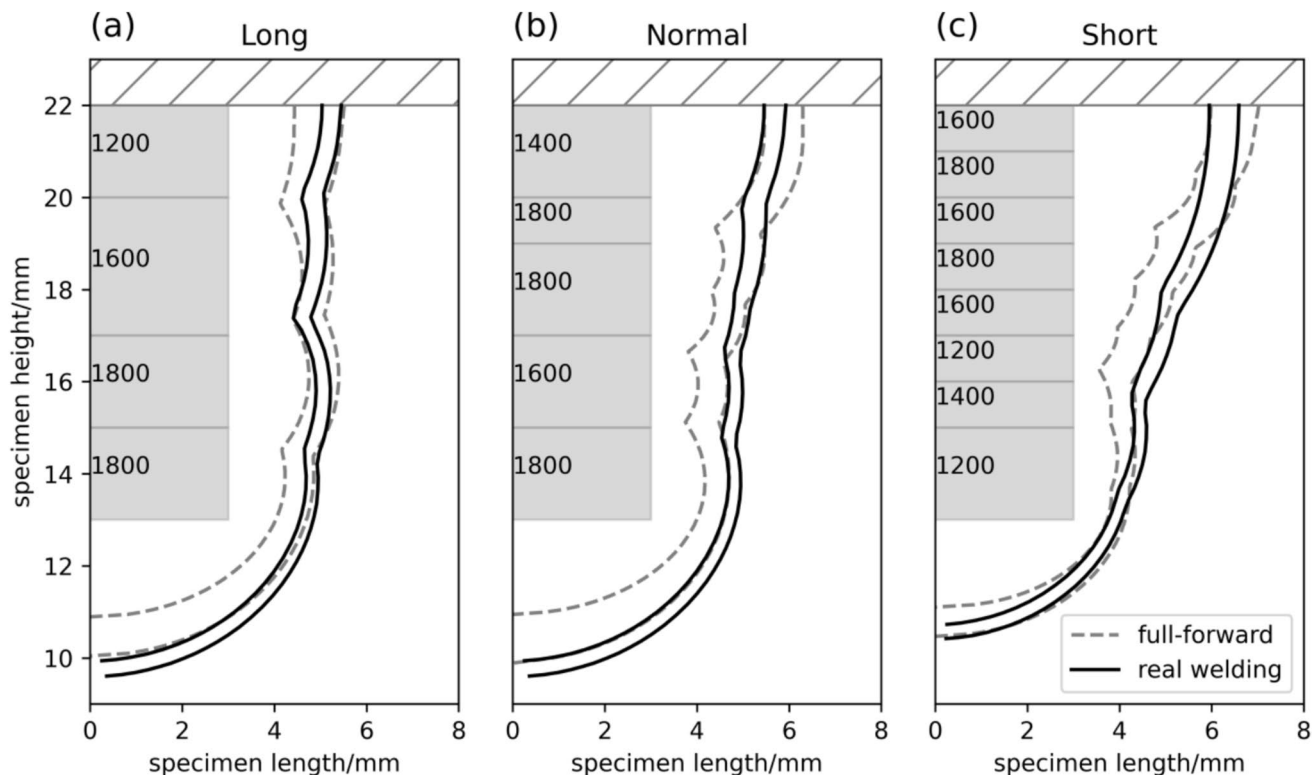


**Fig. 9** Comparison of HAZ cross sectional shape between full-forward and real welding, for (a) Long, (b) Normal and (c) Short condition. Dashed gray lines show the HAZ boundary from real welding and solid black lines show the HAZ shape from full-forward calculation

deformation capability between the base metal and the HAZ, which depends on their elastic and creep deformation parameters. In addition, the temperature and stress dependence of creep rupture life for the HAZ material is also important. In this study, the material properties for the HAZ, both creep deformation and rupture behavior, were obtained from a simulated HAZ that underwent heat treatment to simulate the actual fine-grained microstructure of the actual HAZ region [15]. Although the simulated HAZ was made from 2 1/4Cr–1Mo steel like the base metal, its composition differed slightly. Moreover, actual HAZ regions in multi-pass welding are subjected to multiple thermal cycles, and their resulting microstructures may not be identical to those in the simulated HAZ. Therefore, the difference in material properties between actual and simulated HAZ likely affected the underestimation of rupture life in the creep-only analysis.

In summary, improving the quantitative prediction of creep rupture life requires addressing two key issues: (1) refining the definition of the HAZ region in heat conduction analysis to better match the actual HAZ geometry, and (2) tuning the material properties used in creep damage analysis to improve consistency with experimentally observed behavior.

## 4 Conclusion

Welding conditions to improve the creep performance of weld joints in heat-resistant steels were proposed, and their effectiveness was validated by extracting test specimens from the weld joints and conducting creep tests. The proposed method employed a probabilistic search framework based on an inverse problem, utilizing a tandem Bayesian model. The search space consisted of 1.5 million combinations of welding conditions, varying in layer thickness, number of layers, and heat input. From this space, the optimal welding condition (long-creep-life) was identified. In addition to the proposed long-creep-life condition (Long), a standard condition (Normal) and a short-creep-life condition (Short) were selected. Weld joints were fabricated under these conditions, specimens were extracted, and their creep performance was experimentally compared.

The conclusions are as follows:

- Through optimization using the tandem Bayesian model, it was possible to propose welding conditions that achieved 1.8 times longer rupture life than the longest among the initial conditions, using forward analyses on only a small fraction of the total conditions. The longest-creep-life condition consisted of four layers, with reduced heat input in the final layer. When the surrogate models were appropriately optimized, their ability to propose long-creep-life conditions improved in a stepwise manner.
- The optimized Bayesian linear regression model suggested that favorable HAZ shapes for long-creep-life conditions are smooth and vertically aligned with respect to the tensile axis.
- The results of welding and creep testing under the proposed conditions confirmed that the experimentally observed ranking of rupture life (Long > Normal > Short) matched the model predictions. The HAZ geometries obtained from welding reflected the expected shapes derived from the welding parameters. Furthermore, differences in HAZ shape factors could explain the differences in rupture life, demonstrating that creep rupture life can be controlled via welding conditions mediated through HAZ shape.
- A comparison between forward simulation and creep test results showed that the full-forward model tended to overestimate rupture life, while the creep-only model, based on actual HAZ shapes, tended to underestimate it. These discrepancies were attributed to inaccuracies in reproducing HAZ width and differences in material properties. It was concluded that improving prediction accuracy requires refining the HAZ definition in the heat conduction analysis and tuning the material properties used in creep damage analysis to better match experimental results.

This study experimentally demonstrated the effectiveness of the methodology for identifying welding conditions that achieve long creep life. It combines a sequential numerical simulation—consisting of heat conduction analysis to predict HAZ geometry and creep damage analysis to estimate rupture life—with a tandem Bayesian optimization framework, grounded in the metallurgical understanding of Type IV failure in heat-resistant steel weld joints. The results provide a practical example of how suitable process conditions can be proposed to achieve targeted performance.

Nevertheless, discrepancies were observed between the predicted and experimental creep rupture lives. These discrepancies were attributable to inherent uncertainties in the two forward analyses—the welding heat conduction analysis and the creep damage analysis. Future improvements in prediction accuracy are expected through the refinement of these forward models, particularly by improving the HAZ definition in the heat conduction analysis and optimizing the material parameters used in the creep damage analysis.

## Appendix 1: Parameters for Heat Conduction and Creep Damage Analyses

The parameters for the heat conduction analysis, except for the target welding parameters, were determined as follows. The heat source width  $w$  and heat source depth  $d$  in the



Goldak heat source model were defined as functions of target welding parameters, the heat input  $HV$  (J/mm) and the layer thickness  $DL$  (mm). First, real welding tests were conducted using representative values of  $DL$  and  $HV$ , and the molten zone geometry—defined as the region exceeding the melting point—was identified through cross-sectional observation of weldments. Heat conduction analyses were performed while varying  $w$  and  $d$  to replicate this geometry, and the optimal values of  $w$  and  $d$  were determined accordingly. These were regressed as functions of  $HV$  and  $DL$ , yielding the following equations (1) and (2), where the coefficients  $A_i$  ( $i = 1, 2, 3, 4$ ) and  $B_i$  ( $i = 1, 2, 3, 4$ ) were obtained:

$$w = A_1 \times HV \times DL + A_2 \times HV + A_3 \times DL + A_4 \quad (1)$$

$$d = B_1 \times HV \times DL + B_2 \times HV + B_3 \times DL + B_4 \quad (2)$$

The obtained coefficients  $A_i$  and  $B_i$  are shown in Table 4.

For the other parameters in the heat conduction analysis, the vertical position of the heat source center was set equal to the layer thickness. The welding speed was fixed at 1.667 mm/s, and the heat source length at 2 mm. The remaining parameters for the Goldak heat source model are the welding speed (1.667 mm/s), heat source length (2 mm), front-to-rear heat distribution ratio (1:2), and front-to-rear shape ratio (1:2). They are summarized in Table 4. The thermal properties of the base metal and weld metal were calculated using JMatPro [27], with the chemical compositions of base metal and weld material shown in Table 1.

The parameters used in the creep damage analysis were based on a prior study [15], corresponding to the test conditions in this study, 873 K and 100 MPa. The values used are listed in Table 5. The parameters for both the base metal and weld metal were taken from the base metal, whereas those for the HAZ were taken from the simulated HAZ. The creep deformation law was the Norton-Arrhenius law, and the creep damage model followed the time exhaustion rule using Hudleston stress (details are described elsewhere [23]).

**Table 4** Parameters for equation for heat width (eqn.(A1)), heat depth (eqn.(A2)) and other heat source model parameters

	1	2	3	4
A	$6.159 \times 10^{-4}$	$5.072 \times 10^{-4}$	-1.460	5.076
B	$-4.378 \times 10^{-4}$	$6.341 \times 10^{-4}$	1.145	-0.920
Welding speed	1.667 mm/s			
heat source length	2 mm			
heat source length ratio	1:2			
heat input ratio	1:2			

**Table 5** Parameters for creep damage analysis, minimal creep rate for Norton-Arrhenius law, rupture time and elastic constants

	minimal creep rate		rupture time		elastic constants		misc.
	$\log A_\epsilon$	$n_\epsilon$	$\log A_{TER}$	$n_{TER}$	$Q_{TER}$ (J)	Young's modulus (MPa)	Poisson's ratio
base metal & weld metal	$2.94 \times 10^1$	2.72	$-2.84 \times 10^1$	-2.2	$-3.36 \times 10^5$	$1.56695 \times 10^5$	$2.74 \times 10^{-1}$
simulated HAZ	1.88	4.62	$-1.87 \times 10^1$	-5.4	$-3.55 \times 10^5$	$1.06890 \times 10^5$	

## Appendix 2 Table of welding path thickness configuration and pair numbers

Number of layers	Layer thickness combination whose sum = 9 (mm)	Layer thickness configuration pattern	Layer thickness configuration pattern × heat input pattern	Total
3	3 3 3	1	$1 \times 64 = 64$	64
4	2 2 2 3	$4C1 = 4$	$4 \times 256 = 1024$	4096
	1 2 3 3	$4C2 \times 2C1 = 12$	$12 \times 256 = 3072$	
5	1 2 2 2 2	5	$5 \times 1024 = 5120$	46080
	1 1 1 3 3	$5C2 = 10$	$10 \times 1024 = 10240$	
	1 1 2 2 3	$4C2 \times 5 = 30$	$30 \times 1024 = 30720$	
6	1 1 1 2 2 2	$6C3 = 20$	$20 \times 4096 = 81920$	204800
	1 1 1 1 2 3	$6C2 \times 2C1 = 30$	$30 \times 4096 = 122880$	
7	1 1 1 1 1 3	7	$7 \times 16384 = 114688$	458752
	1 1 1 1 1 2 2	$7C2 = 21$	$21 \times 16384 = 344064$	
8 <sup>*)</sup>	1 1 1 1 1 1 2	8	$8 \times 65536 = 524288$	524288
9	1 1 1 1 1 1 1 1	1	$1 \times 262144 = 262144$	262144
sum				1500224

\*) divide 8 groups for each layer thickness configuration

## Appendix 3

The criteria for excluding damaged elements due to singular stress fields, as well as the method for constructing a classifier to determine whether rupture life can be computed, are explained. From the creep damage analysis results obtained in the forward workflow, time-series data of the damage distribution for all elements at each time step were extracted. At each time point, the set of damaged elements (i.e. damage = 1) within the HAZ was partitioned into connected components, defined as groups of elements that share edges or faces. These connected components were analyzed according to the following criteria to classify rupture types:

- If only connected components not including triple junctions were present: the time of appearance of the component was defined as the rupture life (rupture type: internal rupture).
- If the connected component including a triple junction had a spatial extent not exceeding 0.1 mm from the triple junction, and there also existed another component that did not include a triple junction (non-triple-junction component): the time at which such a non-triple-junction component appeared was defined as the rupture life (rupture type: modified internal rupture, see Fig. 4(a)).
- If no non-triple-junction components were present and a component including a triple junction extended more than 0.1 mm from the junction: it was judged that damage due to singular stress and other causes could not be separated, and rupture life was not determined (rupture type: boundary rupture, see Fig. 4(b)).

Based on these rules, rupture type classification and rupture life estimation were applied to the time-series damage distribution data from the creep damage analysis, and both rupture life and rupture type were recorded. If rupture life could not be determined, the data were excluded from the training dataset. However, rupture type was recorded to prevent redundant recalculation when the same condition was selected again as a candidate.

For screening purposes, a RandomForestClassifier [28] was constructed using the HAZ geometry factors as explanatory variables. The classification target was set such that “internal rupture” or “modified internal rupture” was labeled as 1, and “boundary rupture” as 0. Hyperparameter optimization was performed using GridSearchCV [29] as implemented in scikit-learn. The search space for the hyperparameters of the RandomForestClassifier is shown in Table 6. The timing of classifier training was synchronized with each update of the Bayesian linear regression training dataset.

**Table 6** Parameters range of 10-fold CV (GridSearchCV) for the optimizing of RandomForestClassifier

parameters	GridSearchCV range
n_estimators	1 ~ 7
criterion	“gini”, “entropy”, “log_loss”
max_depth	3 ~ 7
random_state	1 ~ 20
fold	10

**Acknowledgements** The authors are grateful to Mr. Koyo Daimaru (NIMS) for providing programs for calculation of MInt system.

**Author contribution** The research design was proposed by M.D. and H.I. and discussed by all authors. The design of welding conditions, actual welding, specimen preparation and observation were performed by D.A. and K.T., with contributions to the welding condition design made by M.D. and H.I. The optimization method was developed by H.I. under the supervision of K.N., and the calculations and analysis of results were conducted by H.I. under the guidance and discussion with M.D. and H. I. The manuscript and figures were prepared by M.D. and H.I. All authors have given approval to the final version of the manuscript.

**Funding** This work was partly supported by MEXT Program: Data Creation and Utilization Type Material Research and Development Project Grant Number JPMXP1122684766 and Materials Open Platform for Structural Materials-DX, NIMS.

**Data availability** The data that support the findings of this study are available in NIMS Materials Data Repository at <https://doi.org/10.48505/nims.5570>.

## Declarations

**Competing interests** The authors declare no competing interests regarding this manuscript.

**Open Access** This article is licensed under a Creative Commons Attribution 4.0 International License, which permits use, sharing, adaptation, distribution and reproduction in any medium or format, as long as you give appropriate credit to the original author(s) and the source, provide a link to the Creative Commons licence, and indicate if changes were made. The images or other third party material in this article are included in the article's Creative Commons licence, unless indicated otherwise in a credit line to the material. If material is not included in the article's Creative Commons licence and your intended use is not permitted by statutory regulation or exceeds the permitted use, you will need to obtain permission directly from the copyright holder. To view a copy of this licence, visit <http://creativecommons.org/licenses/by/4.0/>.

## References

- Francis JA, Mazur W, Bhadeshia HKDH (2006) Review type IV cracking in ferritic power plant steels. *Mater Sci Technol* 22:1387–1395. <https://doi.org/10.1179/174328406X148778>
- Parker JD, Parsons AWJ (1995) High temperature deformation and fracture processes in 2 1/4Cr-1Mo-1/2Cr 1/2Mo 1/2V weldments. *Int J Press Vessels Piping* 63:45–54. [https://doi.org/10.1016/0308-0161\(94\)00047-M](https://doi.org/10.1016/0308-0161(94)00047-M)
- Ogata T, Yaguchi M (2007) Damage mechanism in weldment of 2.25Cr-1Mo steel under creep-fatigue loading. *Eng Fract Mech* 74:947–955. <https://doi.org/10.1016/j.engfracmech.2006.08.024>
- Li Y, Hongo H, Tabuchi M, Takahashi Y, Monma Y (2009) Evaluation of creep damage in heat affected zone of thick welded joint for Mod. 9Cr-1Mo steel. *Int J Press Vessels Pip* 86:585–592. <https://doi.org/10.1016/j.ijpvp.2009.04.008>
- Ogata T, Yaguchi M (1998) High-temperature strength property evaluation of heat affected zone in boiler weldment parts of 2.25Cr-1Mo steel. *J Soc Mater Sci Japan* 47:253–259. <https://doi.org/10.2472/jsms.47.253>
- Abe F, Tabuchi M (2004) Microstructure and creep strength of welds in advanced ferritic power plant steels. *Sci Technol Weld Join* 9:22–30. <https://doi.org/10.1179/136217104225017107>
- Francis JA, Cantin GMD, Mazur W, Bhadeshia HKDH (2009) Effects of weld preheat temperature and heat input on type IV failure. *Sci Technol Weld Join* 14:436–442. <https://doi.org/10.1179/136217109X415884>
- Parker JD (2013) Factors affecting type IV creep damage in grade 91 steel welds. *Mater Sci Eng A* 578:430–437. <https://doi.org/10.1016/j.msea.2013.04.045>
- Koiwa K, Tabuchi M, Demura M, Yamazaki M, Watanabe M (2019) Prediction of creep rupture time using constitutive laws and damage rules in 9Cr-1Mo-V-Nb steel welds. *Mater Trans* 60:213–221. <https://doi.org/10.2320/matertrans.ME201703>
- Tanner DW, Sun W, Hyde TH (2012) The effect of weld fusion zone angle in a cross-weld specimen under creep. <https://hdl.handle.net/1983/5ef4c48c-7e1f-4e4d-b707-0241aafadc9>. Accessed 24 Dec 2025
- Divya M, Das CR, Albert SK, Goyal S, Ganesh P, Kaul R, Swaminathan J, Murty BS, Kukreja LM, Bhaduri AK (2014) Influence of welding process on type IV cracking behavior of P91 steel. *Mater Sci Eng A* 613:148–158. <https://doi.org/10.1016/j.msea.2014.06.089>
- Hashimoto M, Koyama T, Sato T, Tamura K (1995) Creep damage analysis of welded joints including HAZ softening region. *J Soc Mater Sci Japan* 44:11–15. <https://doi.org/10.2472/jsms.44.11>
- Watanabe T, Tabuchi M, Yamazaki M, Hongo H, Tanabe T (2006) Creep damage evaluation of 9Cr-1Mo-V-Nb steel welded joints showing type IV fracture. *Int J Press Vessels Pip* 83:63–71. <https://doi.org/10.1016/j.ijpvp.2005.09.004>
- Hongo H, Tabuchi M, Watanabe T (2012) Type IV creep damage behavior in Gr.91 steel welded joints. *Metall Mater Trans A* 43A:1163–1173. <https://doi.org/10.1007/s11661-011-0967-6>
- Izuno H, Demura M, Yamazaki M, Tabuchi M, Abe D, Torigata K (2021) Damage model determination for predicting creep rupture time of 2 1/4Cr1Mo steel weld joints. *Mater Trans* 62:1013–1022. <https://doi.org/10.2320/matertrans.MT-MA2020004>
- Abe D, Torigata K, Izuno H, Demura M (2024) Study of analysis method to predict creep life of 2.25Cr-1Mo steel from welding conditions. *Weld World* 68:1297–1311. <https://doi.org/10.1007/s40194-024-01726-4>
- Demura M (2024) Challenges in materials integration. *ISIJ Int* 64:503–512. <https://doi.org/10.2355/isijinternational.ISIJINT-2023-399>
- Minamoto S, Kadohira T, Ito K, Watanabe M (2019) Materials integration system for materials design and manufacturing. *Mater Japan* 58:511–514. <https://doi.org/10.2320/materia.58.511>
- Demura M, Koseki T (2020) SIP-materials integration projects. *Mater Trans* 61:2041–2046. <https://doi.org/10.2320/matertrans.MT-MA2020003>
- Izuno H, Demura M, Yamazaki M, Minamoto S, Sakurai J, Nagata K, Mototake Y, Abe D, Torigata K (2024) Search for high-creep-strength welding conditions considering HAZ shape factors for 2 1/4Cr-1Mo steel. *Weld World* 68:1313–1332. <https://doi.org/10.1007/s40194-024-01727-3>
- Electricité de France (1989–2017) Finite element code\_aster. Analysis of structures and thermomechanics for studies and research. Open source on [www.code-aster.org](http://www.code-aster.org). Accessed 24 Dec 2025
- FrontISTR. GitLab. <https://gitlab.com/FrontISTR-Commons/FrontISTR>. Accessed 13 May 2025

23. Huddleston RL (1985) An improved multiaxial creep-rupture strength criterion. *J Press Vessel Technol* 107:421–429. <https://doi.org/10.1115/1.3264476>
24. Izuno H, Demura M, Tabuchi M, Mototake Y, Okada M (2020) Data-based selection of creep constitutive models for high-Cr heat-resistant steel. *STAM* 21:219–228. <https://doi.org/10.1080/14686996.2020.1738268>
25. Hein VL, Erdogan F (1971) Stress singularities in a two-material wedge. *Int J Fract* 7:317–330. <https://doi.org/10.1007/BF00184307>
26. Ohji K, Kubo S, Nakai Y, Ioka S (1992) Free-edge stress singularity dominated region in bonded dissimilar materials and its disappearance. *J Soc Mater Sci Japan* 41:1389–1395. <https://doi.org/10.2472/jsms.41.1389>
27. Saunders N, Guo Z, Li X, Miodownik AP, Schille JPh (2003) Using jmatpro to model materials properties and behavior. *JOM* 55:60–65. <https://doi.org/10.1007/s11837-003-0013-2>
28. Pedregosa F et al (2011) Scikit-learn: machine learning in Python. *JMLR* 12:2825–2830. <https://doi.org/10.48550/arXiv.1201.0490>
29. Breiman L (2001) Random forests. *Mach Learn* 45:5–32. <https://doi.org/10.1023/A:1010933404324>

**Publisher's Note** Springer Nature remains neutral with regard to jurisdictional claims in published maps and institutional affiliations.